Proceedings of the 17th World Congress
The International Federation of Automatic Control
Seoul, Korea, July 6-11, 2008

A closed-loop approach to reducing scan errors in nanopositioning platforms

S. S. Aphale, B. Bhikkaji and S. O. R. Moheimani *

* *School of Electrical Engineering and Computer Science, The University of Newcastle, Australia, E-mail: {sumeet.aphale, bharath.bhikkaji, reza.moheimani} @newcastle.edu.au*

Abstract: Piezoelectric stack-actuated parallel-kinematic nanopositioning platforms have their first resonant mode at relatively low frequencies and also suffer from nonlinearities such as hysteresis and creep, resulting in a typically low-grade positioning performance. Closed-loop control algorithms have shown the potential to eliminate these problems and achieve robust, repeatable nanopositioning. In this work, the performance of three commonly used damping controllers is compared based on their closed-loop noise characteristics. The best one is combined with an integrator to produce accurate raster scans of large areas while imparting substantial damping to the system and minimizing inherent nonlinearities. A scanning resolution of approximately 8nm, over a $100\mu m \times 100\mu m$ area is achieved.

Keywords: Nanopositioning, resonance damping, tracking, feedback control

1. INTRODUCTION

Advances in nanopositioning directly affect a range of important fields including nanomachining, scanning probe microscopy, microlithography and nanometrology, Fujimasa (1996); Desai et al. (1998); Bhushan (2004). Nanoplatforms have desirable properties such as larger range of motion, greater mechanical robustness, lower cross-coupling between the axes and ease of integration.

The two main factors that limit the performance of nanopositioning platforms are: (i) Resonance and (ii) Nonlinearities. Researchers, Kang and Mills (2005), have proposed techniques to damp the resonant modes of highly resonant systems such as piezoelectric tube nanopositioners. Passive techniques such as shunt damping have been reported by earlier researchers, Fleming and Moheimani (2006). Although, such techniques can deliver acceptable performance, they may need frequent tuning, Niederberger et al. (2004). Resonant control has been applied to damp resonant systems, Pota et al. (2002). These controllers have attractive robustness properties. However, they also have a high-pass profile that may worsen the measurement noise, a main consideration in precise nanopositioning applications. Polynomial-based pole placement control, Goodwin et al. (2001), and Positive Position Feedback (PPF) control, Fanson and Caughey (1990), are some other popular techniques and have been applied to damp the resonant modes of nanopositioning systems such as the piezoelectric tube nanopositioners, Bhikkaji et al. (2007) as well as cantilever beams, Moheimani et al. (2006). These controllers provide robust damping performance under variations in resonance frequencies. They also have a high-frequency roll-off and thus do not excite the unmodeled high-frequency dynamics.

In nanopositioning platforms actuated by piezoelectric stacks, nonlinearities such as hysteresis and creep result in degraded scan performance. Closed-loop compensation of hysteresis and creep is desirable and simple tracking controllers such as an integrator, have shown potential in eliminating the errors due to these nonlinearities, Jung et al. (2001).

Closed-loop nanopositioning schemes are less common than the open-loop architectures due to the low resolution resulting from the fed back sensor noise, see Sebastian and Salapaka (2005). Croft et al. (2001) have proposed open-loop compensation for the vibration as well as nonlinearities in piezoelectric actuators. Researchers have also proposed feedforward techniques to address hysteresis as well as simple filter based compensation techniques to deal with creep in piezoelectrically actuated scanning devices, El-Rifai and Youcef-Toumi (2002). Most techniques are used to obtain scans either for very small ranges (<10 μm) or at low speeds (<1 Hz). We propose a simple yet well-performing closed-loop nanopositioning scheme that results in high-resolution scans of large areas (100μm $\times$ 100μm) at high speeds (4 Hz).

1.1 Objectives

The main objective of this work is to obtain high-resolution closed-loop raster scans using a piezoelectric stack-actuated nanopositioning platform. Section 2 describes the experimental setup and Section 3 gives the details of the system identification and the design algorithms for the three controllers. Based on the noise analysis given in Section 4, the Polynomial-based pole placement controller is deemed most suitable for this specific application. Experimental results are given in Section 5 and Section 6 concludes the paper.

2. EXPERIMENTAL SETUP

The PI-734 nanopositioning platform, used in this work, is a two-axis piezoelectric stack-actuated platform based on

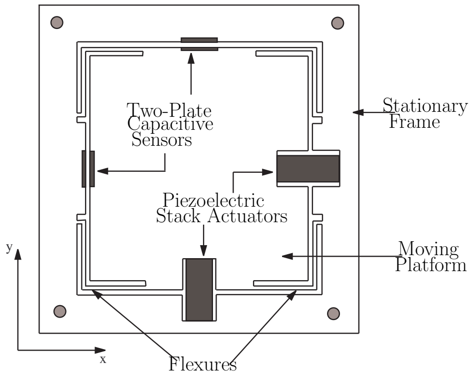

Fig. 1. Working principle of the monolithic XY piezoelectric-stack actuated nanopositioning platform.

a parallel-kinematic design. This design provides mounting independent orthogonality and reduced cross-coupling between the two axes. The platform has a flexure guidance system which eliminates friction and stiction. To increase the range of motion whilst maintaining the sub-nanometer accuracy of the platform, it is equipped with a built-in integrated lever motion amplifier. Each axis of the nanopositioning platform is fitted with a two-plate capacitive sensor that provides a direct position measurement. A simplified diagram of the nanopositioning platform is given in Figure 1. The platform piezoelectric stack actuators take voltage input in the range of 0 V - 100 V for each axis. The resultant motion produced by the platform is within 0 μm - 100 μm. This motion is detected by the two-plate capacitive sensors and fed to a signal conditioning module with an output range of 0 V - 6.7 V. A dSPACE-1005 rapid prototyping system equipped with 16-bit ADC(DS2001)/DAC(DS2102) cards and a sampling frequency of 20 kHz, is used to implement the proposed control strategy.

3. SYSTEM IDENTIFICATION AND CONTROL

The nanopositioning platform is treated as a two-input two-output linear system with inputs u_x and u_y being the voltage signals applied to the piezoelectric stacks in the X and Y directions, respectively, and the outputs d_x and d_y being the corresponding displacements in μm, measured by the capacitive sensor. Here, we set

$$Y(s) \triangleq G(s)U(s), \tag{1}$$

where $U(s)$ is the Laplace transform of $[u_x, u_y]^\top$, $Y(s)$ denotes the Laplace transform of $[d_x, d_y]^\top$, and

$$G(s) = \begin{bmatrix} G_{xx}(s) & G_{xy}(s) \\ G_{yx}(s) & G_{yy}(s) \end{bmatrix} \tag{2}$$

is 2×2 matrix of transfer functions.

It is evident from the plots (Figure 5) that the magnitude of the cross coupling terms $G_{xy}(\mathrm{i}\omega)$ and $G_{yx}(\mathrm{i}\omega)$, at any $\omega > 0$, are less than the direct terms $G_{xx}(\mathrm{i}\omega)$ and $G_{yy}(\mathrm{i}\omega)$, respectively, by about 40 dB [1]. Therefore the cross coupling terms can be neglected and the system is assumed to be decoupled.

[1] The two resonant modes seen in each of the cross-coupling FRFs are due to the mechanical resonant peaks of each individual axis. Therefore, they occur at exactly the same frequencies, i.e. at 410 Hz and 415 Hz, in both the G_{xy} and G_{yx}.

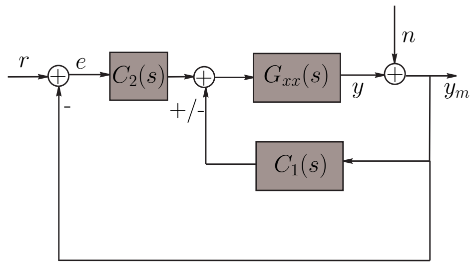

Fig. 2. Closed-loop block diagram with the sensor noise modeled as an output disturbance.

$G_{xx}(\mathrm{i}\omega)$ and $G_{yy}(\mathrm{i}\omega)$, have only one resonant mode in the bandwidth of interest and second order models given by

$$G_{xx}(s) = \frac{k_x}{s^2 + 2\sigma_x\omega_x s + \omega_x^2} + D_x, \tag{3}$$

and

$$G_{yy}(s) = \frac{k_y}{s^2 + 2\sigma_y\omega_y s + \omega_y^2} + D_y, \tag{4}$$

accurately capture the dynamics of the measured FRFs. The parameters of these models are tabulated in Table 1. As the models are of second order their estimation is not difficult, and the details on parameter estimation are omitted.

k_x	8.1532×10^6
$2\sigma_x\omega_x$	6.05×10^1
ω_x^2	6.65×10^6
D_x	-0.13
k_y	8.0023×10^6
$2\sigma_y\omega_y$	5.64×10^1
ω_y^2	6.8×10^6
D_y	-0.13

Table 1. Parameter values of the FRFs $G_{xx}(s), G_{yy}(s), G_{c_{xx}}(s)$ and $G_{c_{yx}}(s)$

3.1 Control Design

As the axes are considered to be decoupled, controllers are designed independently for each axis and the implemented strategy is shown in Figure 2. Here, controller $C_1(s)$ is aimed at damping the resonant mode of $G_{xx}(s)$ (or $G_{yy}(s)$), while $C_2(s)$ is incorporated for tracking the reference signal. In the following, three different control techniques, (*i*) Polynomial-based pole placement control (will be referred to as Polynomial-based control, from now on) (*ii*) PPF control and (*iii*) Resonant control, will be used for obtaining $C_1(s)$. The controllers will be chosen such that all the three damp the resonant peak by approximately the same level. In Section 4, one of the three will be chosen based on their response to sensor noise $n(t)$, see Figure 2 [2].

Polynomial-based controller: In the current context, a Polynomial-based controller is defined by the second order transfer-function

[2] Note that both PPF and Polynomial-based controllers are implemented in positive feedback while the resonant controller is implemented in negative feedback.

$$K_{Poly}(s) \triangleq \frac{\Gamma_1 s + \Gamma_2}{s^2 + 2\xi w s + w^2}, \tag{5}$$

where ξ, w, Γ_1 and Γ_2 are the design parameters. Since the feedback is positive, the transfer-function connecting the output d_x and the input u_x is given by

$$G_{xx}^{(cl)}(s) = \frac{G_{xx}(s)}{1 - G_{xx}(s) K_{Poly}(s)}. \tag{6}$$

For the closed loop system to be well damped it is desirable that its poles are well inside the left half plane. The poles of $G_{xx}(s)$, computed from (3), are $p_\pm = -30.23 \pm \mathrm{i}2578.5$. Here, the desired closed-loop poles are set to

$$P_{1\pm} = P_{2\pm} = -1030.23 \pm \mathrm{i}2578.5,$$

which amounts to placing the closed-loop poles of the system further into the left half plane by 1000 units.

It can be checked that the controller

$$K_{Poly}(s) \triangleq \frac{-499.9s + 3.249.10^6}{s^2 + 4121s + 1.247 \times 10^7}, \tag{7}$$

would render a closed-loop system having poles at P_{1+}, P_{2+}, P_{1-} and P_{2-}. This controller damps the resonant mode of the x-axis by 23 dB.

PPF Controller: A PPF controller is defined by the second order transfer function

$$K_{PPF}(s) = \frac{\gamma_p}{s^2 + 2\eta_p \omega_p s + \omega_p^2}. \tag{8}$$

It is similar to Polynomial-based controller, (5), but without the velocity term Γ_1. As the feedback is positive, the transfer-function connecting the output d_x and the input u_x is as in (6) but with $K_{Poly}(s)$ replaced by K_{PPF}. Here, we aspire for a PPF controller, K_{PPF}, which gives the same level of damping as the controller, K_{Poly}, (7). Since, in (7) $\mid \Gamma 1 \mid << \mid \Gamma_2 \mid$, the effect of Γ_1 is negligible near the low frequency regions. Thus, a PPF controller with Γ_1 set zero in (7) would behave the same way as (7) near the low frequency regions. Thus, Γ_1 is set to zero. The resulting PPF controller given by

$$K_{PPF}(s) \triangleq \frac{3.249.10^6}{s^2 + 4121s + 1.247.10^7}, \tag{9}$$

is stable in closed-loop and delivers the same level of damping as (7).

Resonant Controller: In the current context, resonant controllers can be parametrized as

$$K_{Res}(s) = \frac{\alpha s^2}{s^2 + 2\delta\omega s + \omega^2}. \tag{10}$$

As $K_{Res}(s)$ is targeted to damp the resonant mode of the nanopositioning platform, ω is set to the first resonance frequency of the platform. The values of α and δ are chosen graphically such that the absolute value of the difference h, between the real parts of the corresponding open- and closed-loop poles is minimized. The resultant Resonant controller that imparts the same amount of damping as the Polynomial-based controller is

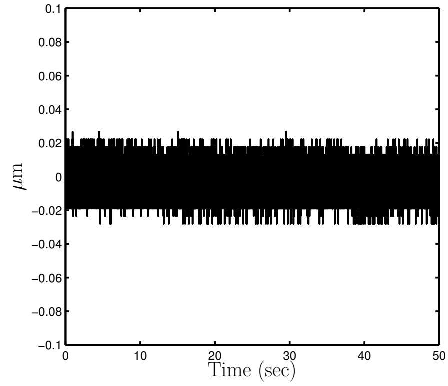

Fig. 3. Noise in the capacitive sensor measurement due to the conditioning electronics.

$$K_{Res}(s) \triangleq \frac{0.3s^2}{s^2 + 3094s + 6.649 \times 10^6}. \tag{11}$$

A statistical analysis of measurement noise and the effects of the three controllers presented here are evaluated. Using this, the controller best suited for nanopositioning applications is identified.

4. MEASUREMENT NOISE

Measurement noise is a major consideration in precision motion at nanometer scales. The recorded sensor output clearly shows the sensor noise as well as the quantization noise, see Figure 3. In our set-up, quantization error is not a major consideration as it is lower (≈1 nm rms) than the actual sensor noise (≈9 nm rms).

The transfer functions relating the actual system output y to the sensor noise n are calculated for the three controllers discussed earlier, see Figure 4. The Polynomial-based controller has a better high-frequency roll-off than the resonant controller and it does not amplify the noise at any frequency as is done by the PPF controller, thus making it ideal for this nanopositioning application.

4.1 Noise Characterization

It can be verified that for the system illustrated in Figure 2, the Laplace transform of the plant output $y(t)$ is equal to

$$\begin{aligned} Y(s) &= \frac{G(s)C_2(s)}{1 + G(s)\left(C_2(s) - C_1(s)\right)} R(s) \\ &\quad - \frac{G(s)\left(C_2(s) - C_1(s)\right)}{1 + G(s)\left(C_2(s) - C_1(s)\right)} N(s) \\ &\triangleq G_r(s)R(s) - G_n(s)N(s), \end{aligned} \tag{12}$$

where $G(s)$ denotes the plant dynamics, $C_1(s)$ and $C_2(s)$ denote the Polynomial-based controller and the integral controller respectively, while $R(s)$ and $N(s)$ are Laplace transforms of the reference signal $r(t)$ and noise $n(t)$ respectively. When operating in open loop, where $Y(s) = G(s)R(s)$, the sensor noise does not disturb the actuation of the plant. However, in closed loop, the sensor noise is fed back into the system, leading to an additional term $Y_n(s) \triangleq G_n(s)N(s)$; the noise response.

The sensor noise $n(t)$ is assumed to be both stationary and ergodic. Thus, its mean, variance and covariances can be

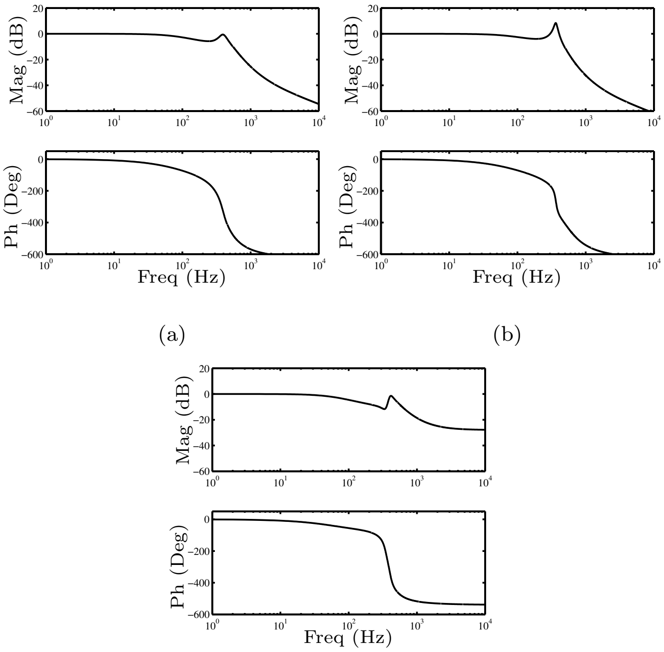

(a) (b) (c)

Fig. 4. Transfer functions relating the actual system output y to the sensor noise n. (a) Polynomial-based controller. (b) PPF controller. (c) Resonant controller.

approximated by the corresponding sample mean, sample variance and sample covariances. The sample mean, $\hat{m}_n$, was approximately 0 and the sample variance, $\hat{\sigma}_n^2$, was approximately $6.2287 \times 10^{-5} \mu m^2$. Since the mean of $n(t)$ is approximately zero, due to linearity, the mean m_{y_n} of the noise response $y_n(t)$ (the inverse Laplace transform of $Y_n(s)$) must also be close to zero, Brown and Hwang (2002).

To determine the variance of $y_n(t)$, the following relationship is used:

$$S_{y_n}(\mathrm{i}\omega) = \mid G_n(\mathrm{i}\omega) \mid^2 S_n(\mathrm{i}\omega), \tag{13}$$

where $S_n(\mathrm{i}\omega)$ and $S_{y_n}(\mathrm{i}\omega)$ are the spectral densities of $n(t)$ and $y_n(t)$ respectively and $G_n(\mathrm{i}\omega)$ is as in (12). The details on how to calculate $S_n(\mathrm{i}\omega)$ and eventually the variance $\hat{\sigma}_{y_n}^2$ from $S_{y_n}(\mathrm{i}\omega)$ are given Brown and Hwang (2002). They are not presented here due to the constraints on the number of pages.

5. EXPERIMENTAL RESULTS USING THE POLYNOMIAL-BASED CONTROLLER

The Polynomial-based controllers for the x and y axes are given by:

$$K_{Poly}(s) \triangleq \frac{-499.9s + 3.249.10^6}{s^2 + 4121s + 1.247.10^7}, \tag{14}$$

and

$$K_{Poly}(s) \triangleq \frac{-490.6s + 3.124 \times 10^6}{s^2 + 4124s + 1.237 \times 10^7}, \tag{15}$$

respectively.

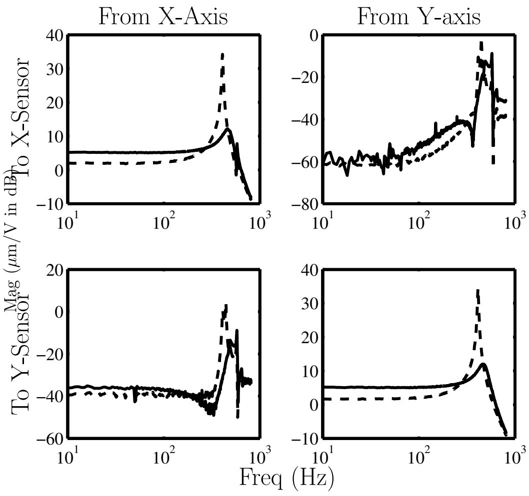

Fig. 5. Open-loop plant(- - -) and closed-loop plant with Polynomial-based controller (—) frequency responses of the two-input two-output nanopositioning platform from displacement output d to platform voltage input u.

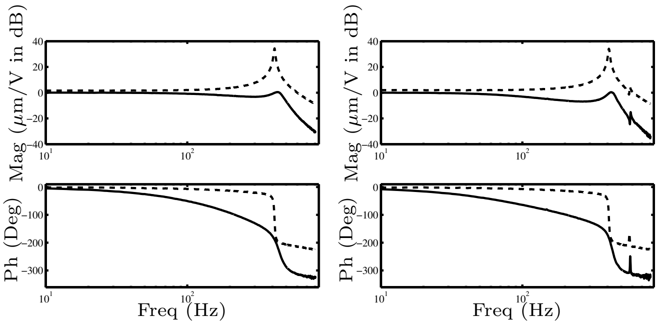

(a) (b)

Fig. 6. Frequency responses for X (a) and Y (b) axes for the open-loop case (- - -) and closed-loop case with Polynomial-based controller+Integral control (—).

The effectiveness of the Polynomial-based controller in damping the resonance of $G_{xx}(s)$ is evaluated both numerically and experimentally. The experimental results agree favourably with the numerical predictions. Figure 5 shows the measured frequency responses of the undamped and damped nanopositioning platform [3].

To eliminate the problems associated with nonlinearities such as hysteresis and creep, a suitable tracking controller is necessary Croft et al. (1999). An integral controller with a gain of 400 was implemented along with the Polynomial-based damping controller, as shown in Figure 2, to result in a well-damped, accurately tracking nanopositioning platform. This resulted in a stable closed-loop system with adequate gain and phase margins. The closed-loop plots are shown in Figure 6.

As mentioned in Subsection 4.1, due to the feedback of the sensor noise, the system output $y(t)$, (12), is not deterministic but random. Having fixed $C_1(s)$ and $C_2(s)$ for both the axes, the variance of the respective outputs can

[3] The cross-coupling FRFs G_{yx} and G_{xy} also show substantial damping at the resonances.

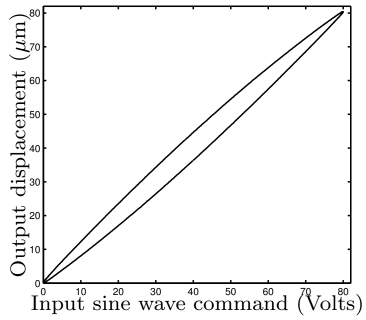

(a)

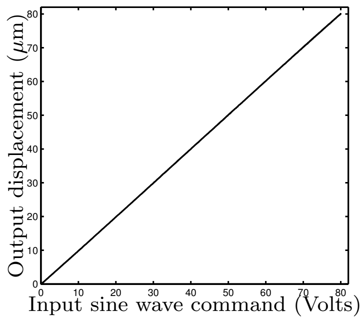

(b)

Fig. 7. Open-loop (a) and closed-loop (b) hysteresis plots for the nanopositioning platform. Input u is a 80 V, 4 Hz sine wave and d is the platform displacement in μm.

be empirically determined using the scheme presented in Subsection 4.1. Avoiding the details involved in calculating $\hat{S}_n(\mathrm{i}\omega_k)$, $G_n(\mathrm{i}\omega_k)$, and $\hat{S}_{y_n}(\mathrm{i}\omega_k)$, the empirical values of the variances along the x and y axes are directly presented. The variances are

$$\sigma^2_{x,y_n} \approx 1.6355 \times 10^{-5} \mu m^2, \tag{16}$$

and

$$\sigma^2_{y,y_n} \approx 1.6230 \times 10^{-5} \mu m^2 \tag{17}$$

along the x and y axis respectively.

5.1 Open- and closed-loop hysteresis and creep evaluation

The platform was excited by a 4 Hz 80 V sine wave and the resultant displacement was measured to give the total deviation from the desired trajectory; the hysteresis loop of the system. Figure 7 (a) shows the open-loop hysteresis plot. Figure 7 (b) shows that the closed-loop control scheme eliminates the nonlinear hysteresis effects almost totally.

The effect of creep on scanning performance is that at two different scan speeds, it produces scans of different magnifications. To test the performance of the open-loop and closed-loop systems for creep, the system is commanded to move instantaneously by 20 μm from its zero initial position at t = 10 s. Figure 8 shows the output

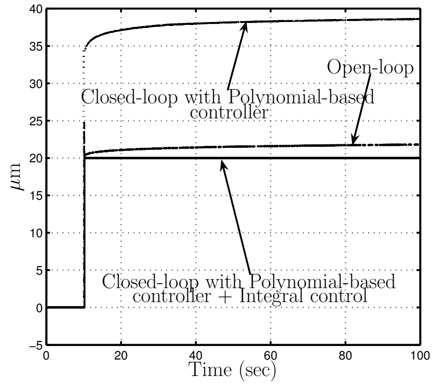

Fig. 8. Open-loop (- - -), Polynomial-based controller-damped closed-loop (. . .) and Polynomial-based controller+integrator closed-loop (—) platform step response (in μm) for a 20 V step command at t=10s.

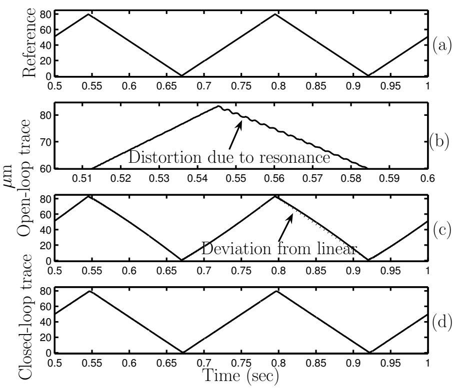

Fig. 9. (a) Reference 4 Hz 80 μm triangle scan. (b) Harmonic distortion due to excitation of resonant mode in open-loop. (c) Complete open-loop scan showing the nonlinear trace due to hysteresis. (d) Closed-loop triangle scan free from errors due to resonance and nonlinearities.

displacement response of the open-loop and closed-loop nanopositioning platform from 0 s to 100 s. As seen clearly from Figure 8, our control scheme has eliminated creep for all practical purposes.

5.2 Raster scan results

A synchronized 4 Hz triangle wave and a staircase waveform were generated to produce the desired raster scan. As shown in Figure 9 (b), this input excites the axis resonance and the output displacement is nonlinear due to hysteresis as seen in Figure 9 (c). The Polynomial-based controller damps the resonant mode and the integrator effectively tracks the 4 Hz input triangle to result in a perfect triangle trace given in Figure 9 (d).

The second axis is given a staircase input and the same performance improvements are observed in closed-loop. The plots presented in Figures 9 and 10 are essentially measurements of the output $y(t)$, (12), along the x and y axes respectively. The measured scan lines of the traced raster pattern are presented in Figure 11. The lines are 62.5 nm apart. The empirical variances given in (16) and (17), imply that the standard deviations σ_{x,y_n} and σ_{y,y_n} are about 4 nm along both the x and y axes. Thus, the

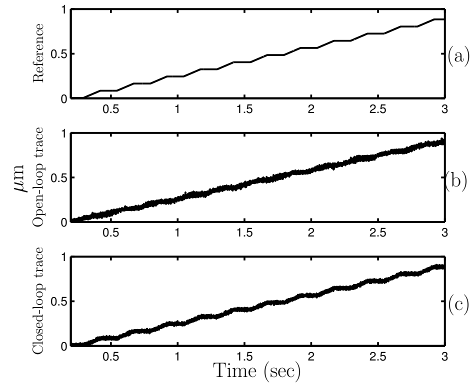

Fig. 10. (a) Reference ramp. (b) Ramp traced in open-loop. (c) Ramp traced in closed-loop.

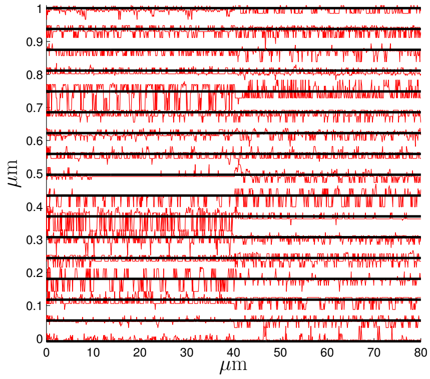

Fig. 11. Measured scan lines (faint) and scan lines obtained using the Kalman estimate (dark) at 62.5 nm from each other.

adjacent scan lines in the raster pattern have to be at least 8 nm (twice the standard deviation) apart, to avoid overlap. With this resolution of 8nm, 12500 scan lines can be produced in a 100 μm scan. In Figure 11, the scan lines are 62.5 nm apart, which is about 15 times the standard deviation. A Kalman estimate of the output $y(t)$ is also plotted to show how accurate the obtained scan is, with respect to the desired scan.

6. CONCLUSIONS

The Polynomial-based controller was identified as the most suitable option for this nanopositioning application. The implemented Polynomial-based controller damps the dominant first resonant mode of the nanopositioning platform by 23 dB. It was further shown that by combining this damping technique with an integral controller, non-linear effects due to hysteresis and creep are minimized and superior tracking performance is achieved. This was demonstrated by tracing a 4 Hz $80\mu\text{m} \times 80\mu\text{m}$ raster scan with a resolution of 62.5nm. Noise analysis suggests a resolution of 8nm is achievable. A more complete noise model, for the covariance data presented Section 4, using the innovations approach would give a better insight into the noise response and eventually would help in achieving a better resolution.

ACKNOWLEDGEMENTS

This work was supported by the Australian Research Council's Center of Excellence for Complex Dynamic Systems and Control.

REFERENCES

B. Bhikkaji, M. Ratnam, A. J. Fleming, and S. O. Reza Moheimani. High-performance control of piezoelectric tube scanners. *Accepted for publication in IEEE Transactions on Control Systems Technology*, May 2007.

B. Bhushan, editor. *Handbook of Nanotechnology.* Springer, 2004.

R. G. Brown and P. Y. C. Hwang. *Introduction to Random Signals and Applied Kalman Filtering.* John Wiley and Sons, New York, USA, 2002.

D. Croft, G. Shedd, and S. Devasia. Creep, hysteresis, and vibration compensation for. piezoactuators: Atomic force microscopy application. *Journal of Dynamic Systems, Measurement, and Control*, 123(1):35–43, March 2001.

D Croft, S Stilson, and S Devasia. Optimal tracking of piezo-based nanopositioners. *Nanotechnology*, 10(2):201 – 208, June 1999.

T. A. Desai, W. H. Chu, J. K. Tu, G. M. Beattie, A. Hayek, and M. Ferrari. Microfabricated immunoisolating biocapsules. *Biotechnology and Bioengineering*, 57:118–120, 1998.

O. M. El-Rifai and K. Youcef-Toumi. Creep in piezoelectric scanners of atomic force microscopes. *Proceedings of the American Control Conference, Anchorage, AK, USA, May*, pages 3777 – 3782, 2002.

J. L. Fanson and T. K. Caughey. Positive position feedback control for large space structures. *AIAA Journal*, 28(4): 717 – 724, 1990.

A. J. Fleming and S. O. R. Moheimani. Sensorless vibration suppression and scan compensation for piezoelectric tube nanopositioners. *IEEE Transactions on Control Systems Technology*, 14(1):33 – 44, January 2006.

I. Fujimasa. *Micromachines: A New Era in Mechanical Engineering.* Oxford University Press, Oxford, UK., 1996.

G. C. Goodwin, S. F. Graebe, and M. E. Salgado. *Control System Design.* Printice Hall International, Inc, 2001.

H. Jung, J. Y. Shim, and D. Gweon. Tracking control of piezoelectric actuators. *Nanotechnology*, 12:14 – 20, 2001.

B. Kang and James K. Mills. Vibration control of a planar parallel manipulator using piezoelectric actuators. *J. Intell. Robotics Syst.*, 42(1):51–70, 2005. ISSN 0921-0296. doi: http://dx.doi.org/10.1007/s10846-004-3028-1.

S. O. R. Moheimani, B. J. G. Vautier, and B. Bhikkaji. Experimental implementation of extended multivariable PPF control on an active structure. *IEEE Transactions on Control Systems Technology*, 14(3):443–455, May 2006.

D. Niederberger, A. J. Fleming, S. O. R. Moheimani, and M. Morari. Adaptive multimode resonant piezoelectric shunt damping. *Smart Materials and Structures*, 18(2): 291–315, October 2004.

H. R. Pota, S. O. R. Moheimani, and M. Smith. Resonant controllers for smart structures. *Smart Materials and Structures*, 11(1):1 – 8, 2002.

A. Sebastian and S. M. Salapaka. Design methodologies for robust nano-positioning. *IEEE Transactions on Control Systems Technology*, 13(6):868 – 876, November 2005.